J. Synchrotron Rad. (1998). **5**, 112–117

In-Situ Hydration Studies Using Multi-Angle Energy-Dispersive Diffraction

S. L. Colston,[a]* S. D. M. Jacques,[a] P. Barnes,[a] A. C. Jupe[a] and C. Hall[b]

[a]Industrial Materials Group, Department of Crystallography, Birkbeck College, Malet Street, London WC1E 7HX, UK, and [b]Schlumberger Cambridge Research, High Cross, Madingley Road, Cambridge CB3 OEL, UK. E-mail: colston@gordon.cryst.bbk.ac.uk

(Received 15 September 1997; accepted 3 December 1997)

A new diffractometer has been built with which energy-dispersive diffraction patterns can be collected simultaneously at different angles. The first use of this system for dynamic (time-resolved) studies – the hydration of cements under various conditions – is reported. It is found that the optimization available with a three-element detector system enables collection of high-quality patterns over a much wider and more effective range of reciprocal space, and this yields improved and new information on the hydration processes.

Keywords: energy-dispersive diffraction; hydration; cements.

1. Introduction

With the wider availability and improved performance of synchrotron X-ray sources, energy-dispersive diffraction (EDD) has become an ideal technique for *in-situ* studies when rapid pattern collection and/or difficult environmental cell designs are crucial. There are many recent examples of its use in the fields of solid-state chemistry (Barnes, 1991; Barnes *et al.*, 1996), hydrothermal synthesis (He *et al.*, 1992; Clark *et al.*, 1995; Lewis *et al.*, 1995), ceramics (Turrillas *et al.*, 1995), cement hydration (Barnes *et al.*, 1992, 1996) and tomography (Hall, Barnes, Cockcroft *et al.*, 1996). Until now, EDD has been practiced using an ED detector at a single scattering angle, 2θ, whose choice is invariably based on a compromise (Hausermann & Barnes, 1992) between factors involving the required d-spacing range, the intensity *versus* photon-energy spectrum of the source, X-ray absorption by the sample, and the geometric component to the diffraction pattern resolution (the 'cot θ effect'). The well known disadvantage of EDD is its relatively poor overall pattern resolution which can result in excessive overlaps between the diffraction peaks. We have sought to alleviate these problems by building an energy-dispersive diffractometer for station 16.4 of the Daresbury SRS (Clark, 1996), in which three ED detectors are positioned, each with their individual collimators and differing 2θ values, so as to share the burden of effective reciprocal-space coverage. In this paper we report the first use of such multi-angle EDD for dynamic *in-situ* studies.

2. Three-element energy-dispersive diffractometer

The main engineering features of this diffractometer have been detailed elsewhere (Barnes *et al.*, 1998). Fig. 1 gives a schematic representation of the basic X-ray optics and an illustration of the problems of alignment with respect to the diffracting volume seen by each detector. The main features are (*a*) the angular separations between each ED detector are fixed at just under 3° since this usually provides a set of three overlapped d-spacing ranges that is appropriate for most studies; (*b*) the goniometer moves the three ED detectors, associated collimators and final slits, together as a whole unit so that all three 2θ values can be varied quickly with the same separation maintained; (*c*) the performance of this system for *in-situ* work is very dependent on alignment of the three-element unit and so the nature of this aspect is briefly explained.

The fixed geometry of the conventional EDD method has the great advantage that the whole of the diffraction pattern can be attributed to the same diffracting volume element, termed a 'lozenge' (Hausermann & Barnes, 1992), which is defined by the intersection of the incident

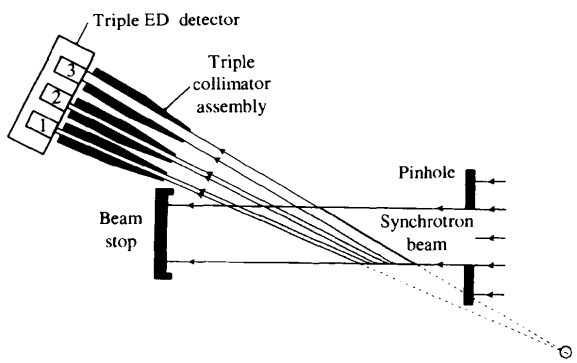

Figure 1
Schematic figure illustrating formation of the three diffraction lozenges, these being defined by the intersection of the input and diffracted/collimated X-rays. The illustration is of a misaligned configuration in which the three lozenges do not overlap.

and diffracted/collimated X-ray paths. The definition and positioning of this lozenge can be put to advantage (Jupe *et al.*, 1996; Hall, Barnes, Billimore *et al.*, 1996; Hausermann & Barnes, 1992) as a means of deliberately identifying the part of the sample (surface, interior *etc.*) from which diffraction is desired. In the case of a three-element system, there are three such lozenges (Fig. 1) and it is obviously desirable in most cases that they should coincide. The following three alignment conditions need to be satisfied: (i) that the centres of all three lozenges are coincident, (ii) that this centre also coincides with the required part of the sample, and (iii) that this centre is also coincident with the goniometer axis. Confirmation of such alignment can be achieved by substituting, for the intended sample, a fine (vertical) capillary containing a reference powder (*e.g.* talc) which acts as a sample position definer. Fig. 2 shows a typical pre-aligned result, obtained by moving the reference sample while collecting total diffracted intensity on all three ED detectors; the FWHM of each peak is a measure of the length of the lozenges as seen by each detector along the incident beam direction, and the degree of separation of the peaks is an indication of the current misalignment. When the diffractometer is fully aligned, all three peaks overlap and remain overlapped during rotation of the whole three-element unit on the goniometer arm. One can then be satisfied that multi-element diffraction patterns correspond essentially to the same *in-situ* volume element. We now present the first two examples of *in-situ* time-resolved data collected using a multi-angle EDD diffractometer.

3. Multi-angle EDD patterns from an industrial cement sample

Fig. 3 shows the EDD patterns obtained in 300 s from an oilwell cement with the detectors at nominal 2θ angles of 3,

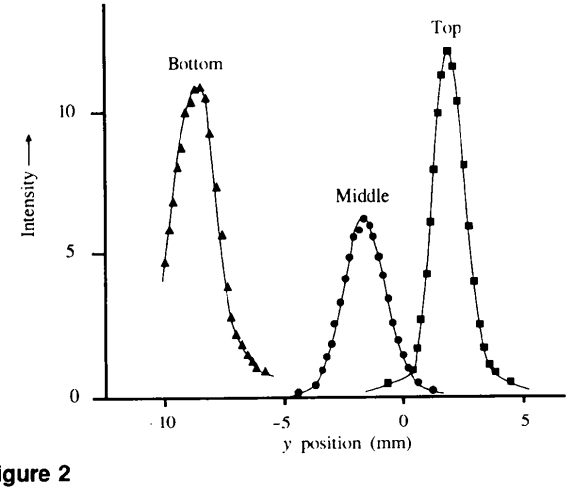

Figure 2
Location of the three diffraction lozenges of the multi-angle ED diffractometer along the X-ray beam (y) direction, using a talc powder sample in a capillary (total EDD intensity in arbitrary units). The plot shows a typical pre-aligned configuration with the top and bottom lozenges displaced from each other by more than 10 mm. In an aligned state the three peaks would be coincident.

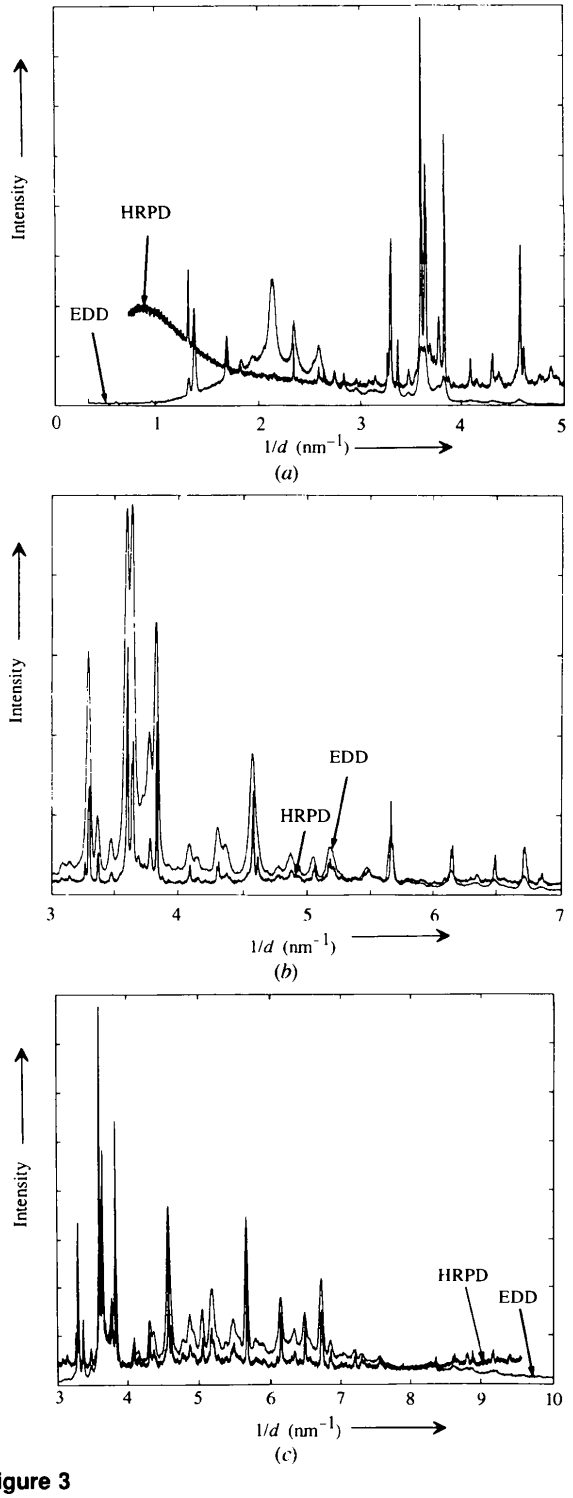

Figure 3
High-quality multi-angle EDD patterns (EDD-16.4) for a commercial (Dyckerhoff) oilwell cement (prior to water addition) compared with synchrotron angle-scanning data (HRPD-2.3) on a common reciprocal ($1/d$) scale. The multi-angle EDD diffractometer is set with 2θ angles of (*a*) 3.04 (bottom), (*b*) 5.84 (middle) and (*c*) 8.75° (top), and the data were collected in 300 s on station 16.4 of the SRS using a cylindrical PEEK sample holder (internal diameter 8 mm; external diameter 12 mm). The high-resolution angle-scanning data were collected over 4 h (0.01° steps) on station 2.3 of the SRS at a wavelength of 1.200 Å. The comparison amply demonstrates the excellent quality of the EDD data and the benefits of the multi-angle EDD method.

6 and 9°. By plotting these three patterns on a common, reciprocal ($1/d$) scale, the overlap and ranges may be easily inspected and the EDD patterns compared with data collected over 4 h from a high-resolution angle-scanning powder diffractometer (station 2.3 of the SRS). This provides an instructive comparison: virtually all peaks in the high-resolution data (HRPD) can be accounted for in one or more of the multi-angle EDD patterns except that in a very few cases a doublet in the HRPD data cannot be properly resolved, the clearest case being at $1/d = 4.6\ \text{nm}^{-1}$ (middle detector). At low angles the HRPD data suffer from well known problems of glancing incidence (a background rise when $1/d < 2.5\ \text{nm}^{-1}$) whereas the equivalent EDD data give one additional peak at $2.14\ \text{nm}^{-1}$ which arises from the PEEK EDD sample holder. The advantage of multi-angle EDD data is striking, producing an effect analogous to a 'movable magnifying glass' since the high-intensity part of the X-ray spectrum falls into different $1/d$ regions in each EDD pattern. For example, the set of multiple-EDD peaks at 3.6–3.9 nm^{-1} is low in intensity and poorly resolved in Fig. 3(*a*), yet is intense and well resolved in Fig. 3(*b*); similarly, the longer d-spacing EDD peaks ($1/d < 3\ \text{nm}^{-1}$) are only visible in Fig. 3(*a*) while the shorter d-spacing EDD peaks ($1/d > 6\ \text{nm}^{-1}$) are 'magnified' in Fig. 3(*c*). Although on equivalent terms, the resolution of the HRPD pattern, typically $\Delta 2\theta = 0.12°$, is several times better than the equivalent EDD pattern resolutions [typically, a 0.4 keV FWHM in Fig. 3(*c*) would be equivalent to an angle-scanning $\Delta 2\theta$ of 0.38°], it would seem that the EDD resolutions are well matched to the cement under study: diffraction patterns from multi-phase cementitious materials are notoriously complex yet we can satisfy our identification and intensity needs simply by choosing the best from the three EDD patterns.

4. Time-resolved multi-angle EDD from cements undergoing high-temperature hydration

We report on results from studies of two hydration systems: an oilwell cement hydrated under autoclave conditions and a synthetic analogue of a Portland cement phase. In each case additional time-resolved information can be extracted by the use of more than one ED detector.

4.1. *Autoclave hydration of an oilwell cement to 425 K*

Oilwell cements (Nelson, 1990; Bensted, 1989) are Portland cements manufactured with a low tricalcium aluminate content. In oilwell operations, cement slurries frequently reach temperatures of 423 K (in geothermal wells sometimes as high as 523 K) and so one of the principal aims is to prevent premature setting of cement under these conditions, prior to proper placement. We have reproduced a typical oilwell schedule (temperature ramp of 293 to 423 K in 30 min, then held at 423 K) in a sealed autoclave EDD cell (He *et al.*, 1992; Hall, Barnes, Cockcroft *et al.*, 1996) for a simple oilwell 'Dyckerhoff' cement/water slurry using the same cement as shown in Fig. 3. A detailed description of the hydration sequence can be extracted from just the raw time-resolved EDD patterns obtained from the three detectors (Fig. 4). Standard cement chemistry shorthand is used throughout (C = CaO; S = SiO_2; A = Al_2O_3; F = Fe_2O_3; H = H_2O; s = SO_3).

4.1.1. *Anhydrous cement.* Prior to reaction with water, the cement EDD patterns consist of many peaks from the unreacted calcium silicate (C_3S, C_2S), alumino-ferrite

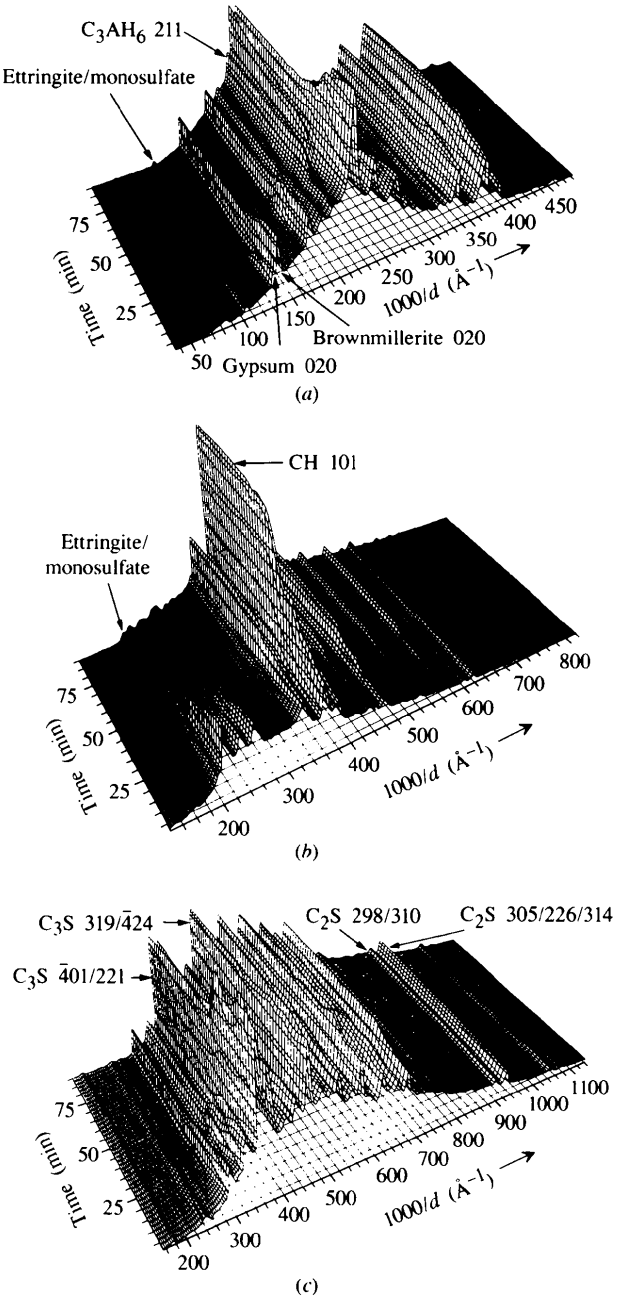

Figure 4
Time-resolved multi-angle EDD patterns showing an oilwell Dyckerhoff cement hydrating under autoclave conditions up to 423 K: (*a*) bottom detector ($2\theta = 3.04°$); (*b*) middle detector ($2\theta = 5.84°$); (*c*) top detector ($2\theta = 8.75°$). Some principal phases/peaks are indicated.

(C_4AF) and gypsum (CsH_2) phases, of which some are indicated in Figs. 4(*a*) and 4(*c*).

4.1.2. *Gypsum/bassanite.* After *ca* 20 min (about 373 K) the gypsum, CsH_2, transforms to bassanite, $CsH_{0.5}$, which is then consumed after *ca* 30 min. This event is best seen with the bottom detector (gypsum 020 peak at $1000/d$ = 130 $Å^{-1}$; bassanite 200 peak at $1000/d$ = 167 $Å^{-1}$, but overlapping with a C_3S 201 peak at $1000/d$ = 169 $Å^{-1}$).

4.1.3. *Brownmillerite hydration.* At ambient temperatures, this phase [stoichiometric formula C_4AF; see also §4.2 below] normally hydrates slowly but under autoclave conditions its consumption accelerates markedly after 25 min (>398 K) as best seen from the 020 peak in the bottom detector ($1000/d$ = 137 $Å^{-1}$).

4.1.4. *Tricalcium aluminate hexahydrate.* The appearance of this phase, C_3AH_6, was a somewhat unexpected result, being formed after 25 min and seen best by its 211 peak appearing as a shoulder on the CH 001 peak (see §4.1.5) on the bottom detector ($1000/d$ = 195 $Å^{-1}$). Its formation appears to be correlated with the loss of brownmillerite (§4.1.3), from which it is known to hydrate, then remaining to the end of the autoclave cycle (90 min). It would appear that this is the first *in-situ* observation of this phase forming under these timescales and conditions and is consistent with published DTA evidence (Ramachandran & Beaudoin, 1976).

4.1.5. *Calcium hydroxide.* The growth of calcium hydroxide, CH, is often considered to mark the end of a 1–3 h dormant hydration stage under ambient conditions. Under these autoclave conditions the CH growth commences after just 25 min and continues to grow to the end (90 min), the commencement appearing to be correlated with the simultaneous loss of gypsum (§4.1.2). It is best seen with the 001 peak in the bottom detector ($1000/d$ = 202 $Å^{-1}$) and the 101 peak in the middle detector ($1000/d$ = 380 $Å^{-1}$) in spite of some overlap with three C_3S peaks ($1000/d$ = 359 $Å^{-1}$).

4.1.6. *Ettringite/monosulfate.* This concerns the well known decomposition reaction of calcium sulfoaluminate hydrate, ettringite $C_3A.3Cs.H_{32}$, to monosulfate, C_3A. Barnes *et al.*, 1996), Fig. 4 being the first display of such data obtained under autoclave conditions. The ettringite and monosulfate peaks are small and partially overlapped with themselves and other peaks (ettringite 100, 110, 104 and 114 peaks at $1000/d$ = 104, 180, 213, 258 $Å^{-1}$; monosulfate 003 and 006 peaks at $1000/d$ = 105, 210 $Å^{-1}$); nevertheless the full data show that the transformation takes place from 15 to 35 min, commencing at *ca* 358 K, though a residual fraction of ettringite appears to remain up to 423 K (Jupe, 1997).

4.1.7. *Tobermorite.* This is a crystalline calcium silicate hydrate, $C_5S_6H_5$, which forms under autoclave curing conditions (Polak *et al.*, 1990). It is not readily visible in the raw data during the early stages of formation, but can be detected by multiple peak-fitting analysis on the 101 and 110 peaks ($1/d$ = 182 and 323 $Å^{-1}$) within the bottom detector patterns.

The main outcome from this study is as follows. We note that EDD appears to be the only method available today by which the bulk transformation of individual mineral phases can be observed in real time under realistic hydrothermal conditions, generating unique information on the chemistry of the cement hydration process (Luke *et al.*, 1995): this is the first comprehensive analysis of cement hydration under an operational oilwell time–temperature schedule (ramp from 293 to 423 K in 30 min) and we can see that the information from two or more EDD detectors is complementary, thereby providing an extremely detailed picture of the first 30 min of autoclave hydration. The results show clearly that the overall hydration process consists of several stages marked by the often sudden appearance and disappearance of particular hydrate/mineral phases. This provides a framework from which one will now be able to study how set-modifying additives perturb and retard the course of cement hydration under geothermal conditions.

4.2. *Hydration of synthetic brownmillerites*

Brownmillerite has the stoichiometric formula C_4AF and is one of the four principal phases occurring in Portland cements, where it occurs with a wide range of substitutions (Bergstrom *et al.*, 1992). As part of a study into its hydration and structural properties, brownmillerite has

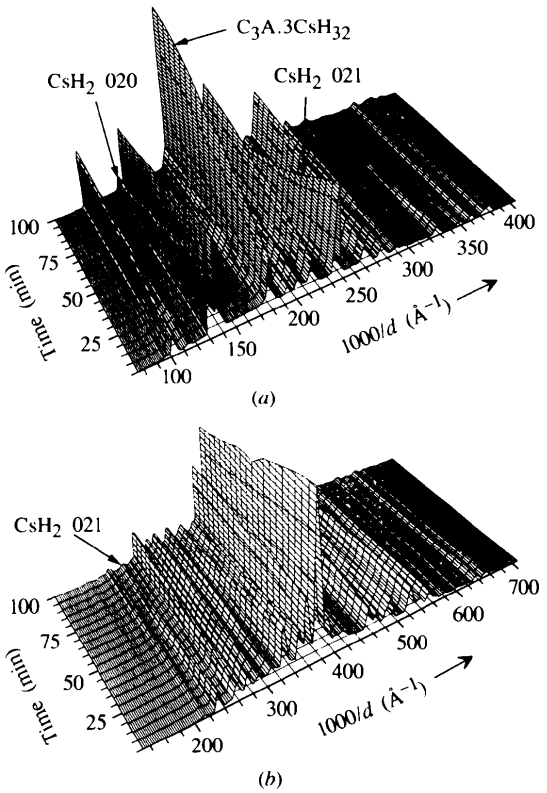

Figure 5
Time-resolved multi-angle EDD patterns showing a synthetic brownmillerite cement phase hydrating at temperatures ramped from 303 to 323 K in 30 min, then held at 323 K: (*a*) bottom detector (2θ = 2.52°); (*b*) middle detector (2θ = 5.28°). Some principal peaks are indicated.

been synthesized (Jupe, 1997) with varying Mg/Si substitutions. In saturated lime water a mixture of stoichiometric pure brownmillerite and gypsum hydrates straightforwardly to form ettringite ($C_3A.3Cs.H_{32}$) according to

$$C_4AF + 3CsH_2 + 29H \xrightarrow{CH} C_3A.3Cs.H_{32} + FH_3.$$

Fig. 5(*a*) contains the main features of this hydration sequence during the temperature ramp from 303 to 323 K, as seen by the bottom detector: the loss of gypsum, CsH_2, throughout the whole 100 min is evident from the diminishing 020 and 021 peaks at $1000/d$ = 132 and 234 Å^{-1}, respectively; some ettringite is already present at the start but grows further as seen best by the 110 peak at $1000/d$ = 179 Å^{-1} and also by the 100 and 104 peaks at $1000/d$ = 104 and 213 Å^{-1}, respectively. We can use this type of information to gain a quantitative view of the rates of hydration: for example, in Fig. 6 we show the rate of loss of gypsum (intensities obtained from Gaussian-fitting of 020 gypsum peaks and corrected for beam decay) for four independent experiments covering two temperature profiles (303–323 K; 303–353 K) and two brownmillerites (stoichiometric C_4AF; Mg/Si-doped C_4AF). This shows, as expected, that the hydration rates increase with temperature but also that pure brownmillerite hydrates more rapidly than the doped forms.

The middle detector (Fig. 5*b*) does not add any further significant information regarding this chemical sequence of events. However, since we are able to monitor a given diffraction peak on two detectors at different 2θ angles, we have a means of comparing the X-ray scattering/absorption by the sample at two different energies. If we assume that the net chemical composition of the sample remains constant and that the sample is homogeneous and with no adverse preferred orientation, then this in principle can yield information about density changes, $\rho(t)$, in the sample with time. The intensities at time t for a given reflection in two detectors, at respective energies E_1 and E_2, will be of the form

$$I_{E_1}(t) = k_1\rho(t)\exp[-a_1\rho(t)],$$

$$I_{E_2}(t) = k_2\rho(t)\exp[-a_2\rho(t)],$$

where the constants k_i and a_i represent unit (per depth and density) scattering and absorption contributions for the reflection at an energy E_i. If we take the natural logarithm of the ratio of the intensities at the two energies, then

$$\ln[I_{E_1}(t)/I_{E_2}(t)] = \ln(k) - a\rho(t),$$

where $k = k_1/k_2$ and $a = a_1 - a_2$.

Thus, changes in this ln(ratio) with time reflect changes in the sample density $\rho(t)$. For example, in Fig. 7 we plot the variation of $\ln(I_{31\ keV}/I_{66\ keV})$ for the gypsum 021 peak during hydration as captured in the bottom (at 66 keV) and middle (at 31 keV) detectors. For the lower temperature sequence (to 323 K) a slow (inverse-sigmoidal) drop in sample density with hydration time is indicated. For the higher temperature ramp (to 353 K) the drop in density is, as expected, much more rapid and then levels off after 30–40 min; this is quite convincing since 30–40 min is also around the time of set (also seen in Fig. 7 by the plateau in ettringite production) after which we indeed expect density changes to be negligible. One could, in principle, take this analysis further by calibrating the constants, a, k, from known density points (*e.g.* at the beginning and end of a hydration sequence) in order to

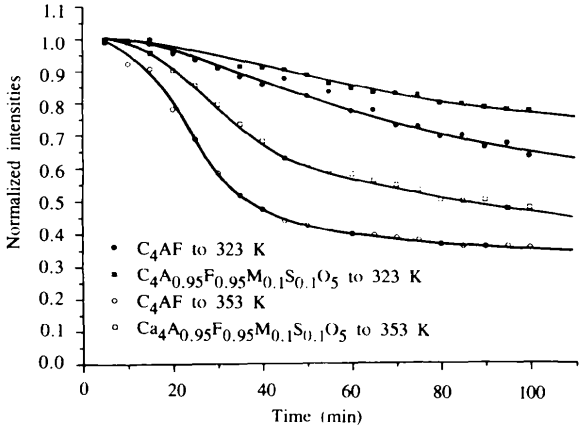

Figure 6
Comparison of the hydration rates of brownmillerite as indicated by the loss of gypsum (021 peak at d = 4.28 Å). This shows, as expected, that hydration rates increase (*i.e.* faster loss of gypsum) with temperature but more notably that the doped form in each case hydrates more slowly than the pure form.

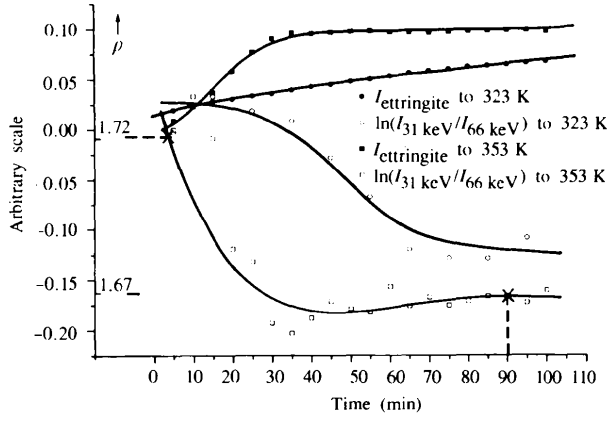

Figure 7
Plots of $\ln(I_{31\ keV}/I_{66\ keV})$ (open circles/squares) *versus* time for the gypsum 021 peak, as obtained from the bottom and middle detectors; these reflect the changes in sample density with hydration time for which the drop is, as expected, more rapid with the higher-temperature sequence (ramp to 353 K). Also included are the growth curves for the ettringite product for both sequences (filled circles/squares, corrected for beam decay and plotted on arbitrary scales) to show that the time periods over which the densities change convincingly coincide with the main periods of growth in each case. The crosses inserted at 5 and 90 min indicate the two calibrating density point measurements performed for the 303–353 K experiment, thereby providing a scale for absolute density estimates, ρ (g cm^{-3}), throughout the whole hydration sequence.

derive absolute density values during the sequence. We have been able to do this in a repeat of the 303–353 K hydration experiment within a graduated glass-tube reaction vessel: light paraffin of known density (0.838 g cm^{-3}) is used to make up known ambient volumes; the cement density can then be calculated from the weight differences, yielding values of 1.72 (±0.01) and 1.67 (±0.01) g cm^{-3} at 5 and 90 min, respectively. Inserting these points into the plot (Fig. 7; 303–353 K) provides a scale for absolute density estimates during the whole hydration sequence, and this represents a further potential advantage from the use of multi-angle EDD.

We see several important outcomes from this particular study. Firstly, it represents the first *in-situ* X-ray diffraction study of brownmillerite hydration and the first comparison of its hydration kinetics for differing temperatures and doping. The results confirm the trend that synthetic brownmillerite hydrates more rapidly than its (impure) Portland cement counterpart. But further, we can see (Fig. 6) that the Mg/Si doping actually retards hydration rates, the retardation if anything increasing with temperature. This result contrasts markedly with the situation for calcium silicate/Portland cements where it has been long known that doping tends to increase hydration rates. Finally, the results present an initial showcase for the need to consider the effect of density changes. Virtually all published quantitative work on EDD ignores this effect, even to the point of erroneously attributing differing growth-curve shapes to the various reflections of the same product, rather than realising these could be simply due to differing absorption-energy dependencies. This multi-angle approach now provides a way to check these assumptions independently; they show that the density/absorption effect can be significant.

5. Conclusions

A three-element energy-dispersive diffractometer has been assembled and aligned so as to enable simultaneous collection of EDD patterns at three angles, thereby effecting a fuller and more optimized coverage of reciprocal space. The system has now been benchmarked on demanding materials: Portland/hydraulic cements in both static and hydrating modes. The quality of the EDD patterns is well matched to cement studies with little or no diffraction information being lost on account of resolution; the multiple diffraction sets enable a far more detailed analysis of the hydration sequences, including an indication of changes in sample density and absorption, this being a hitherto neglected aspect of energy-dispersive diffraction analysis. These improvements are so substantial that we predict this multi-angle mode will become the norm, replacing the traditional single-angle energy-dispersive diffraction method.

We wish to acknowledge the EPSRC for financial support and synchrotron beamtime, CLRC Daresbury Laboratory for considerable assistance with the multi-angle EDD diffractometer, Schlumberger Cambridge Research and Daresbury Laboratory for CASE-studentship support, and British Gas, Schlumberger CR and Castle Cement for financial assistance.

References

Barnes, P. (1991). *J. Phys. Chem. Solids*, **52**, 1299–1306.
Barnes, P., Clark, S. M., Hausermann, D., Henderson, E., Fentiman, C. H., Rashid, S. & Muhamad, M. N. (1992). *Phase Transit.* **39**, 117–128.
Barnes, P., Jupe, A. C., Colston, S. L., Jacques, S. D., Hall, C., Grant, A., Rathbone, T., Miller, M., Clark, S. M. & Cernik, R. J. (1998). *Nucl. Instrum. Methods Phys. Res. B*, **134**, 310–313.
Barnes, P., Turrillas, X., Jupe, A. C., Colston, S. L., O'Connor, D., Cernik, R. J., Livesey, P., Hall, C., Bates, D. & Dennis, R. (1996). *J. Chem. Soc. Faraday Trans.* **92**, 2187–2196.
Bensted, J. (1989). *World Cem.* **20**, 346–357.
Bergstrom, T. B., Hall, C. & Scrivener, K. L. (1992). *Adv. Cem. Res.* **4**, 141–147.
Clark, S. M. (1996). *Nucl. Instrum. Methods Phys. Res. A*, **381**, 161–168.
Clark, S. M., Nield, A., Rathbone, T., Flaherty, J., Tang, C. C., Evans, J. S. O., Francis, R. J. & O'Hare, D. (1995). *Nucl. Instrum. Methods Phys Res. B*, **97**, 98.
Hall, C., Barnes, P., Billimore, A., Jupe, A. C. & Turrillas, X. (1996). *J. Chem. Soc. Faraday Trans.* **92**, 2125–2129.
Hall, C., Barnes, P., Cockcroft, J. K., Jacques, S. D. M., Jupe, A. C., Turrillas, X., Hanfland, M. & Hausermann, D. (1996). *Anal. Commun.* **33**, 245–248.
Hausermann, D. & Barnes, P. (1992). *Phase Transit.* **39**, 99–115.
He, H., Barnes, P., Munn, J., Turrillas, X. & Klinowski, J. (1992). *Chem. Phys. Lett.* **196**, 267–273.
Jupe, A. C. (1997). PhD thesis, London University, UK.
Jupe, A. C., Turrillas, X., Barnes, P., Colston, S. L., Hall, C., Häusermann, D. & Hanfland, M. (1996). *Phys. Rev. B*, **53**, R14697–14700.
Lewis, D. W., Sankar, G., Catlow, C. R. A., Carr, S. W. & Thomas, J. M. (1995). *Nucl. Instrum. Methods Phys. Res. B*, **97**, 44.
Luke, K., Hall, C., Jones, T. G. J., Barnes, P., Lewis, A. C. & Turrillas, X. (1995). *Proc. Soc. Petrol. Eng. Int. Symp. Oilfield Chem.* **28958**, 137–144.
Nelson, E. B. (1990). *Well Cementing; Developments in Petroleum Science*, No. 28, edited by E. B. Nelson. Amsterdam: Elsevier.
Polak, E., Munn, J., Barnes, P., Tarling, S. E. & Ritter, C. (1990). *J. Appl. Cryst.* **23**, 258–262.
Ramachandran, V. S. & Beaudoin, J. J. (1976). *J. Mater. Sci.* **11**, 1893–1910.
Turrillas, X., Barnes, P., Gascoigne, D., Turner, J. Z., Jones, S. L., Norman, C. J., Pygall, C. F. & Dent, A. J. (1995). *Radiat. Phys. Chem.* **45**, 491–508.